Gene Networks that Compensate for Crosstalk With Crosstalk

Müller et al.

A

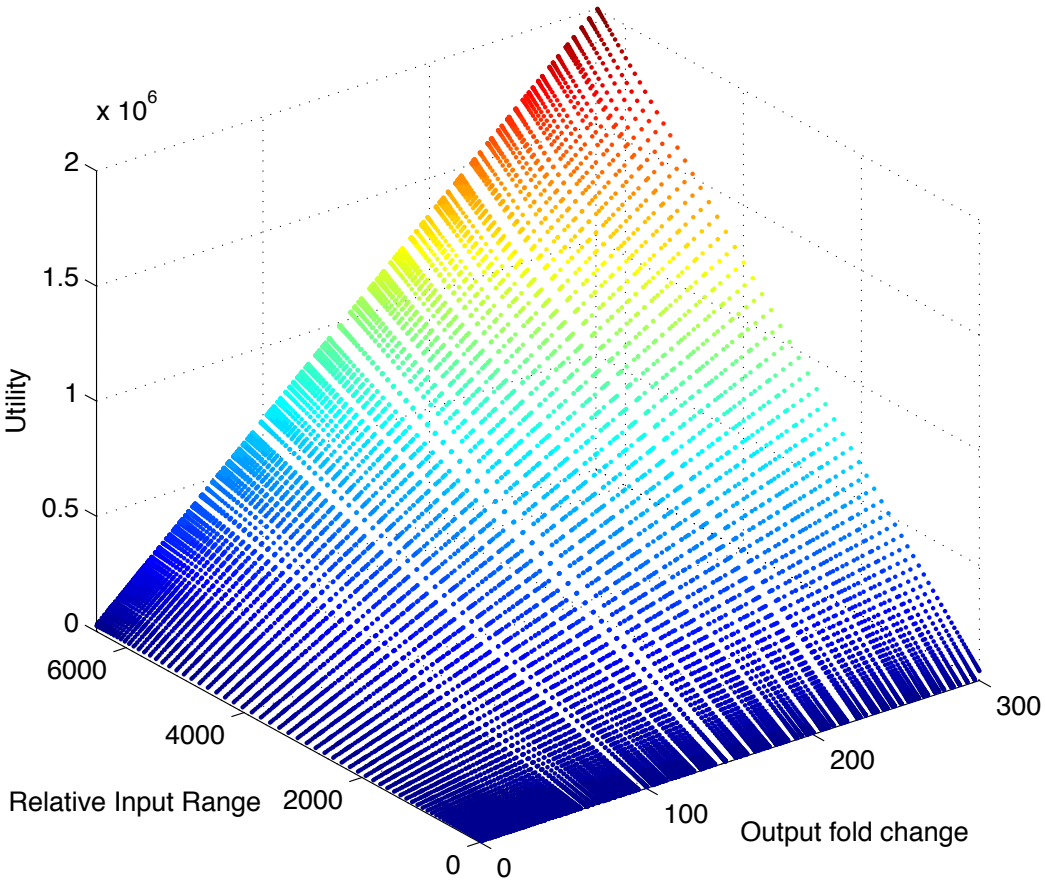
x 10^6
2
1.5
1
0.5
0
Utility
6000
4000
2000
0
Relative Input Range
0
100
200
300
Output fold change

B

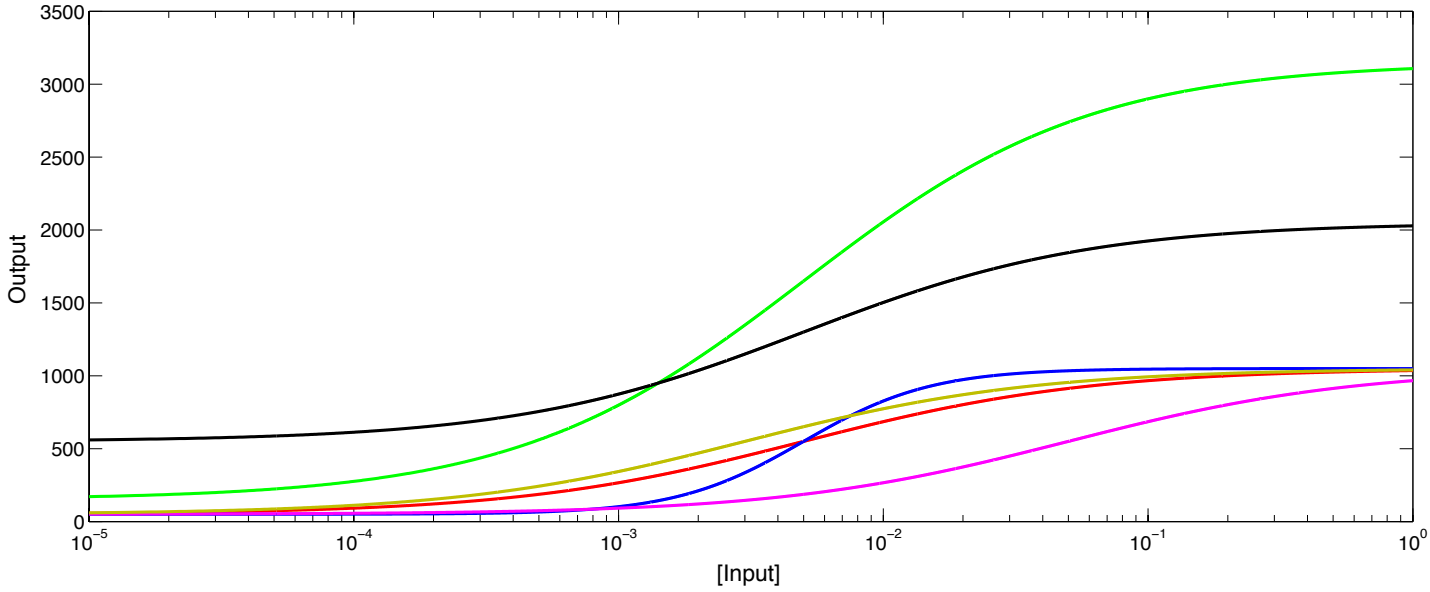
3500
3000
2500
2000
1500
1000
500
0
Output
10^-5
10^-4
10^-3
10^-2
10^-1
10^0
[Input]

C

	1) Red	2) Blue	3) Green	4) Black	5) Purple	6) Yellow
bmax	1000	1000	3000	1500	1000	1000
C	50	50	150	550	50	50
K_d	0.005	0.005	0.005	0.005	0.05	0.003
n	0.8	1.8	0.8	0.8	0.8	0.8
Output Fold Induction	21	21	21	3.73	21	21
Relative Input Range	243	11.49	243	243	243	243
Utility	5103	241.29	5103	906.39	5103	5103

Supplementary Figure 1 | The behavior of the utility metric with different parameters in hypothetical Hill curves. (A) The utility metric was simulated in Matlab over a range of *Bmax*, *C,* and *n* values. *Bmax* ranged from 1000 to 30256.5. *C* ranged from 100.2 to 1000.7. *n* ranged from .5 to 1.5. **(B)** Hill equations with shifted basal and maximum gene expression, K_d, and *n* were simulated in Matlab and **(C)** their utility values were calculated. The red and blue functions differ in the Hill coefficient, *n*. The red and green functions differ in their *C* and *bmax* values but have the same output fold-induction and same utility. The black function is shifted vertically relative to the red function, giving the same difference between *bmax* and *C*, but a lower output fold-induction and utility. The yellow function is shifted to lower K_d relative to the red function, and the purple function is shifted to a higher K_d relative to the red function, but all three functions have the same utility.

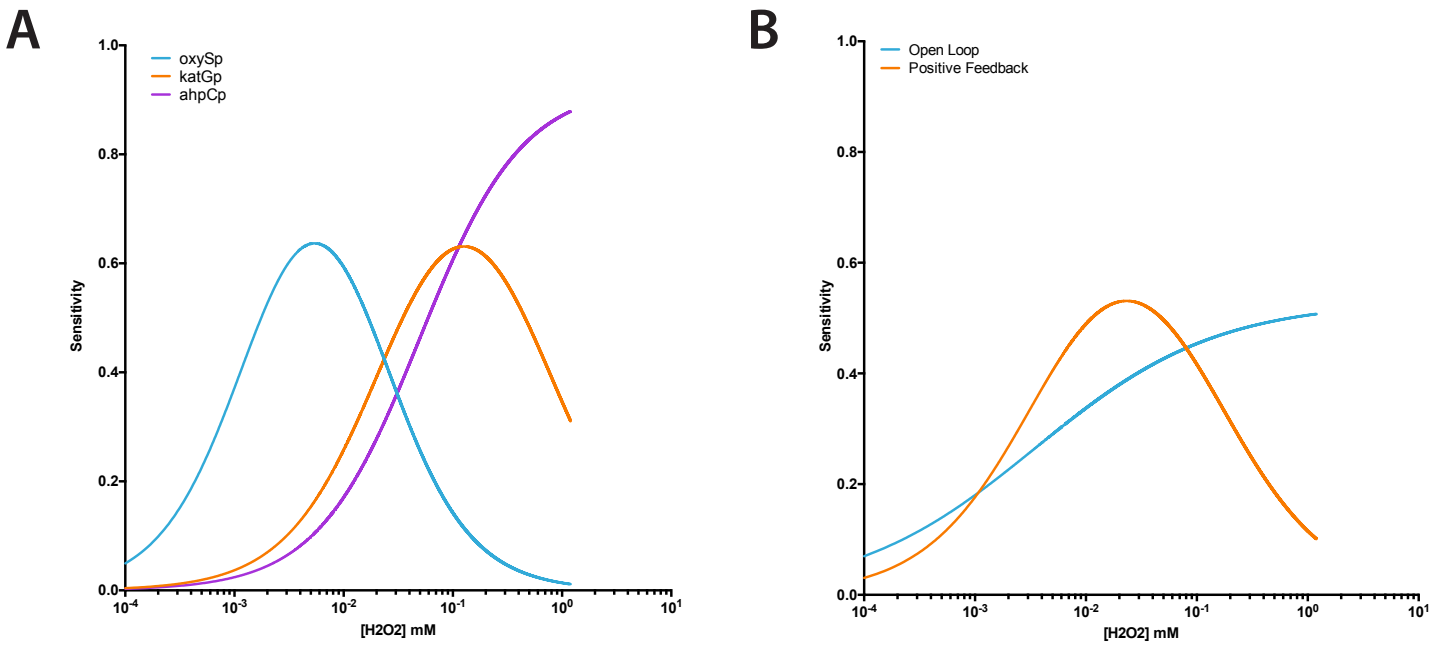

Supplementary Figure 2 | Sensitivities for different H_2O_2-sensing circuits. (A) The sensitivity of the circuits in Fig. 1A was calculated from the Hill equations plotted in Fig. 1B. **(B)** The sensitivity of the circuits in Fig. 1D and 1E was calculated from the Hill equations plotted in Fig. 1F. The sensitivity was calculated as in (1)**:**

$$S(x) = \frac{\frac{\partial y}{y}}{\frac{\partial x}{x}}$$

A

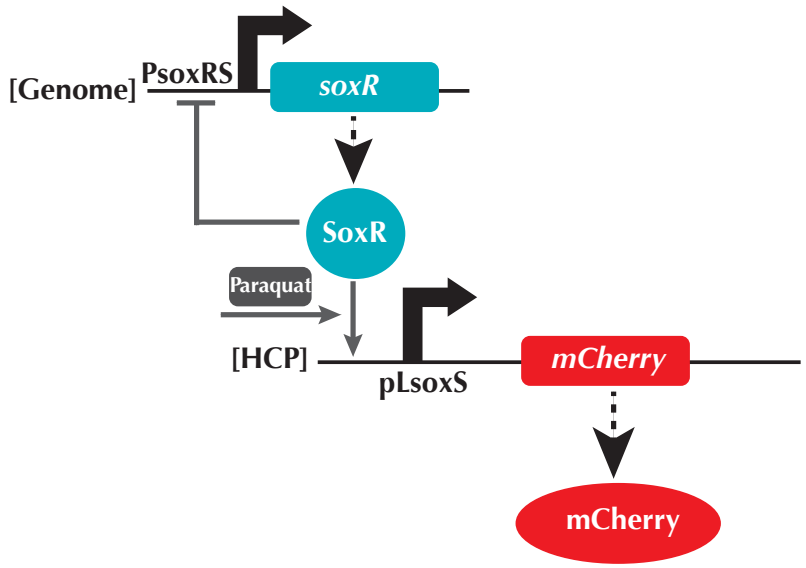

B

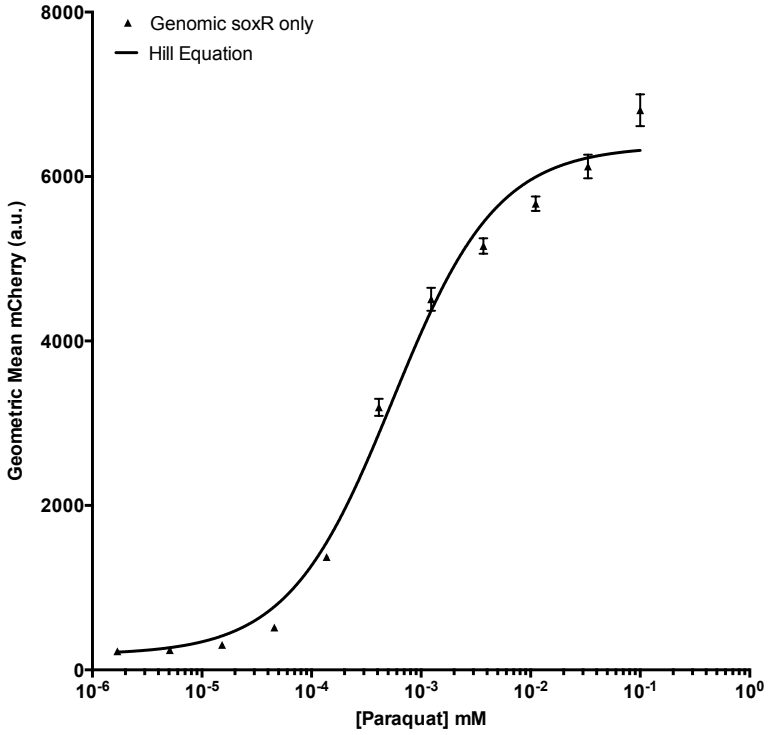

Supplementary Figure 3 | Genomic *soxR* circuit for paraquat sensing. (A) The genomic *soxR* circuit. *SoxR* is expressed from the genome and negatively regulates its own expression (2). *mCherry* expression is controlled by the pLsoxS promoter on a HCP. **(B)** The empirical paraquat-mCherry transfer function for the genomic soxR circuit. The line is a Hill function fit. The errors (s.e.m.) are derived from three biological replicates and flow cytometry experiments, each involving 30,000 events. Source data are provided as a Source Data file.

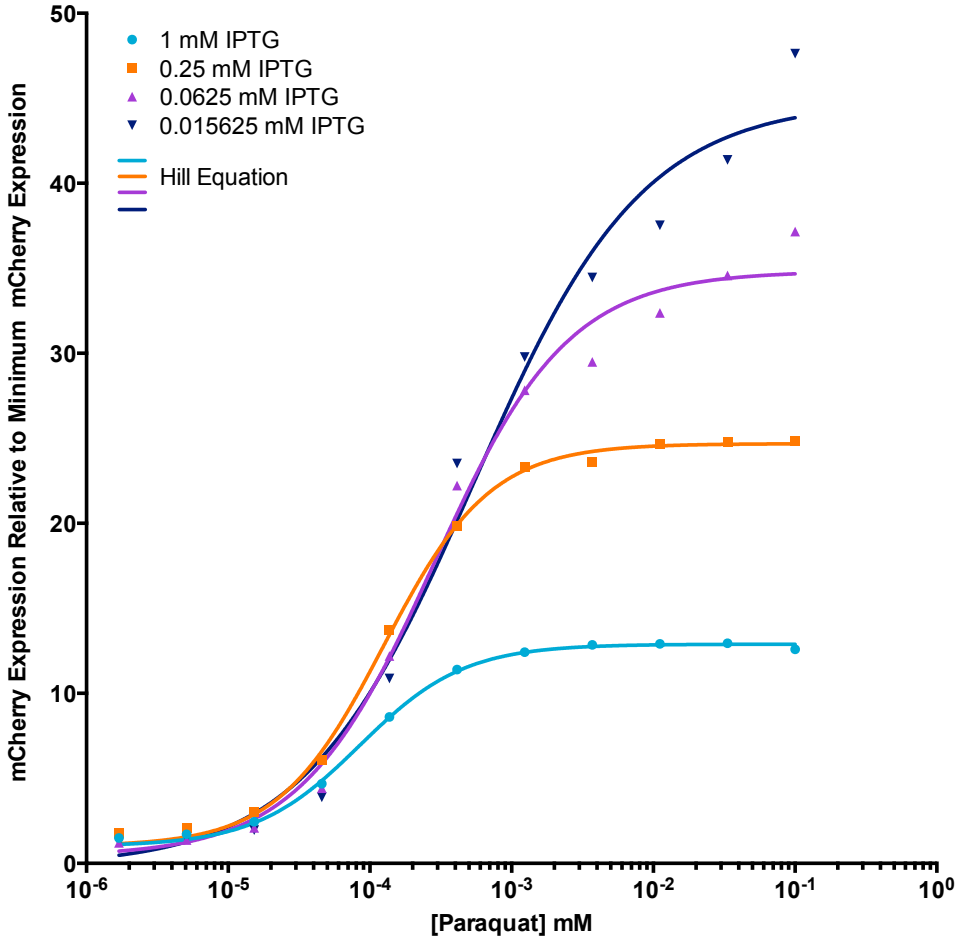

Supplementary Figure 4 | Normalized mCherry expression for the IPTG-controlled paraquat sensing circuit in Figure 2E. mCherry expression across a range of paraquat levels was normalized to mCherry expression at zero paraquat for the circuits and data in Figs. 2E and 2F. Lower IPTG concentrations increased the output fold-induction and input dynamic range.

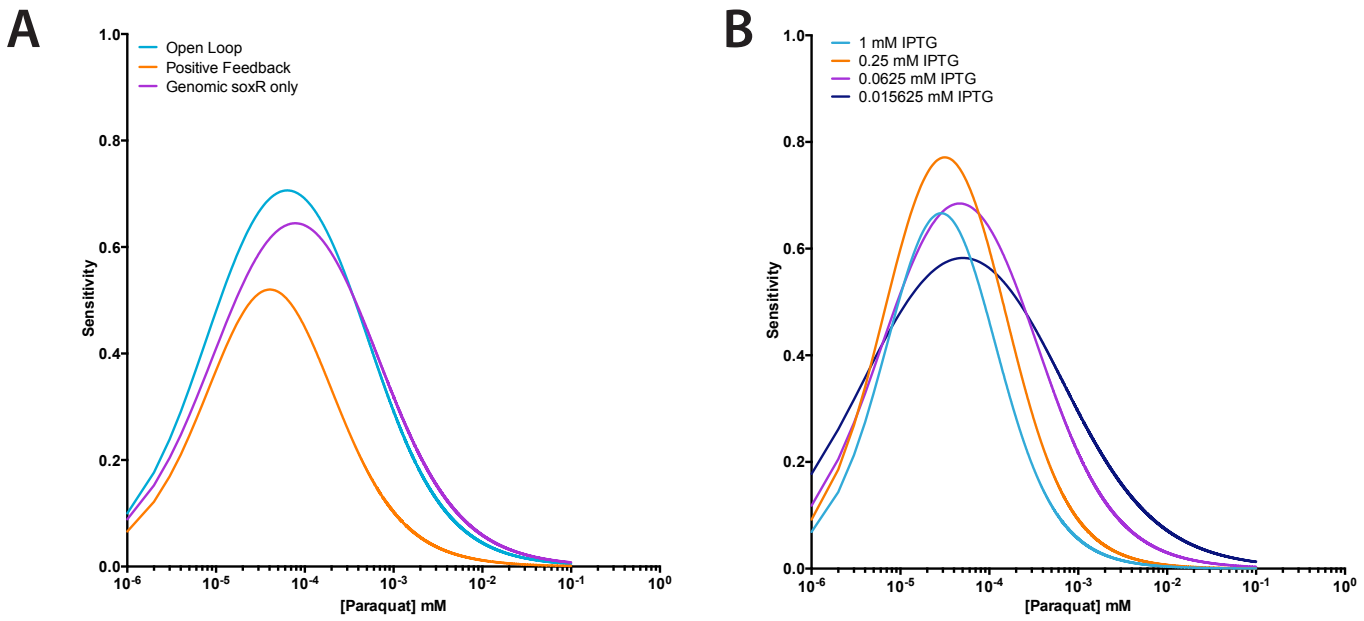

Supplementary Figure 5 | Sensitivities for different paraquat-sensing circuits. (A) Sensitivities of the circuits in Figs. 2A, 2B, and Supplementary Fig. 3A, calculated from the Hill curves plotted in Fig. 2C or Supplementary Fig. 3B. **(B)** Sensitivities of the circuits in Fig. 2E, calculated from the Hill curves plotted in Fig. 2F.

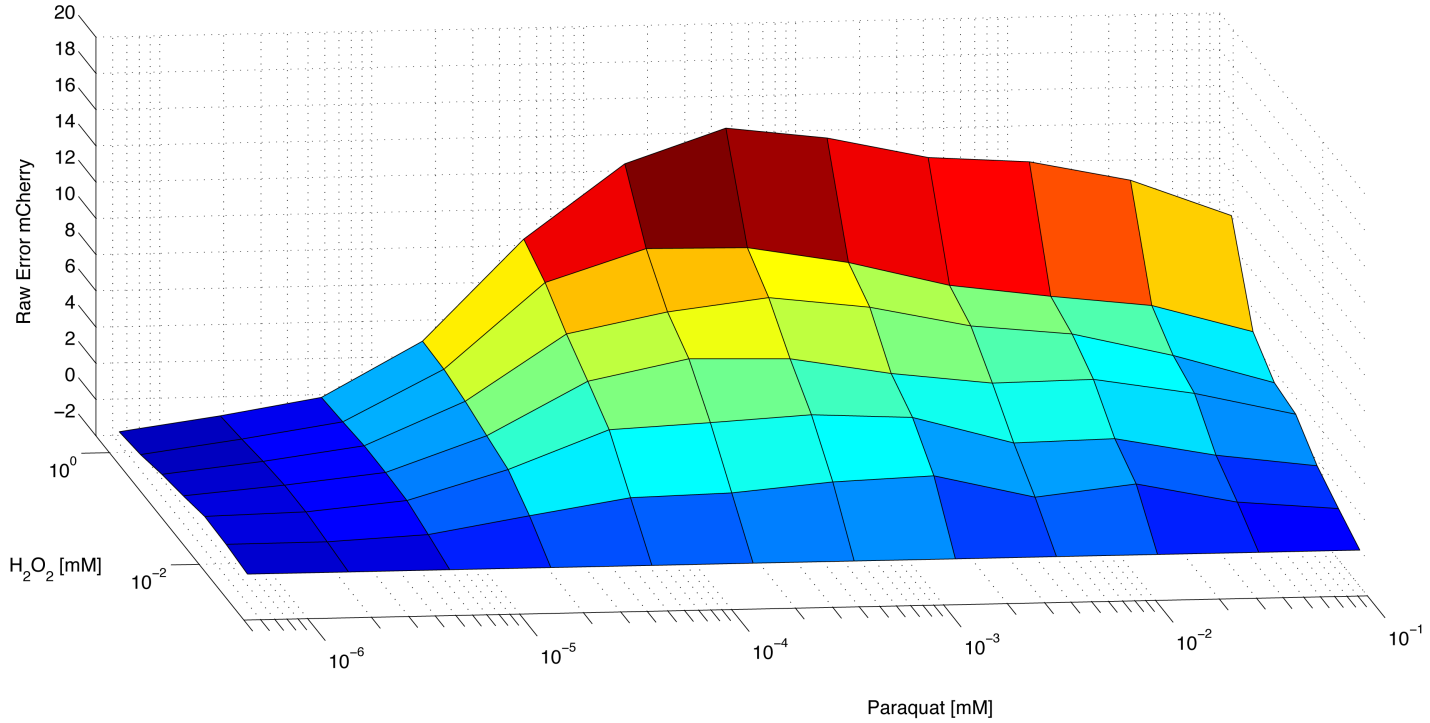

Supplementary Figure 6 | Raw mCherry error for the first iteration of the dual-sensor circuit (Fig. 3A) based on the data in Fig. 3B. The data shown is the mean of the raw error calculated from each experimental replicate and is thus different from that shown in Supplementary Note 2. The lowest concentrations of paraquat and H_2O_2 tested were zero, but are plotted as non-zero numbers so as to be shown on the logarithmic axes.

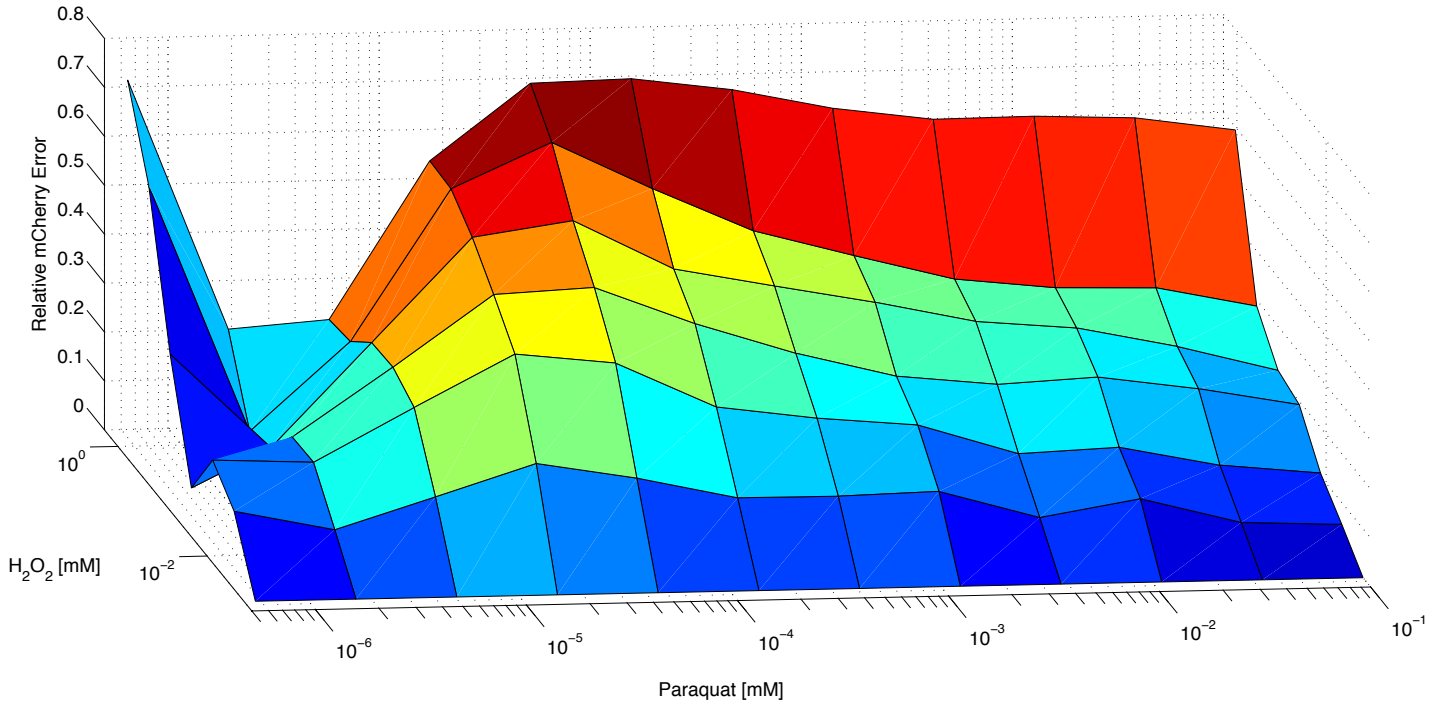

Supplementary Figure 7 | Relative mCherry error for the first iteration of the dual-sensor circuit (Fig. 3A) based on the data in Fig. 3B. The data shown is the mean of the relative error calculated from each experimental replicate and is thus different from that shown in Supplementary Note 2. The lowest concentrations of paraquat and H_2O_2 tested were zero, but are plotted as non-zero numbers so as to be shown on the logarithmic axes.

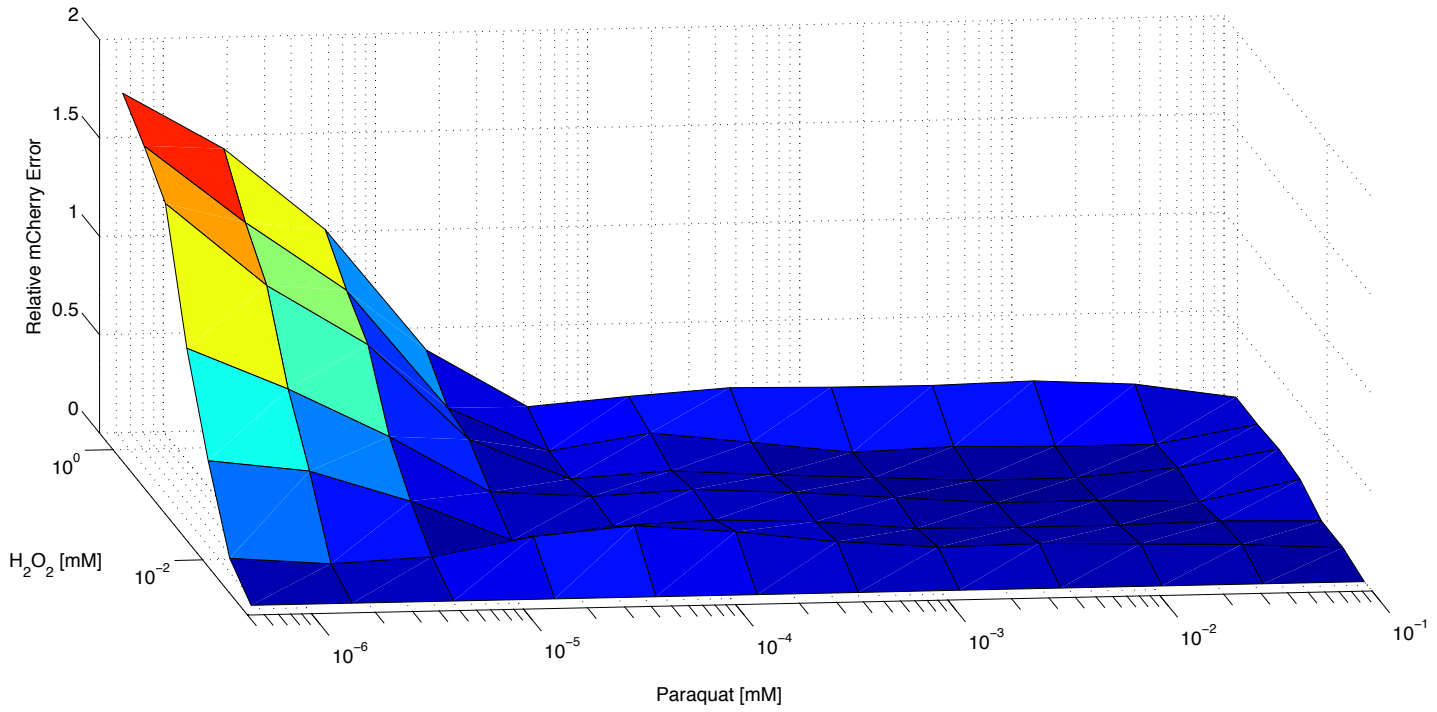

Supplementary Figure 8 | Relative mCherry error for the dual-sensor circuit with the analog compensation circuit (Fig. 3C) based on the data in Fig. 3D. Crosstalk is reduced at high concentrations of paraquat, but is higher at low concentrations of paraquat compared to the initial dual-sensing strain (Supplementary Fig. 7). The data shown are the mean of the relative error calculated from each experimental replicate. The lowest concentrations of paraquat and H_2O_2 tested were zero, but are plotted as non-zero numbers so as to be shown on the logarithmic axes.

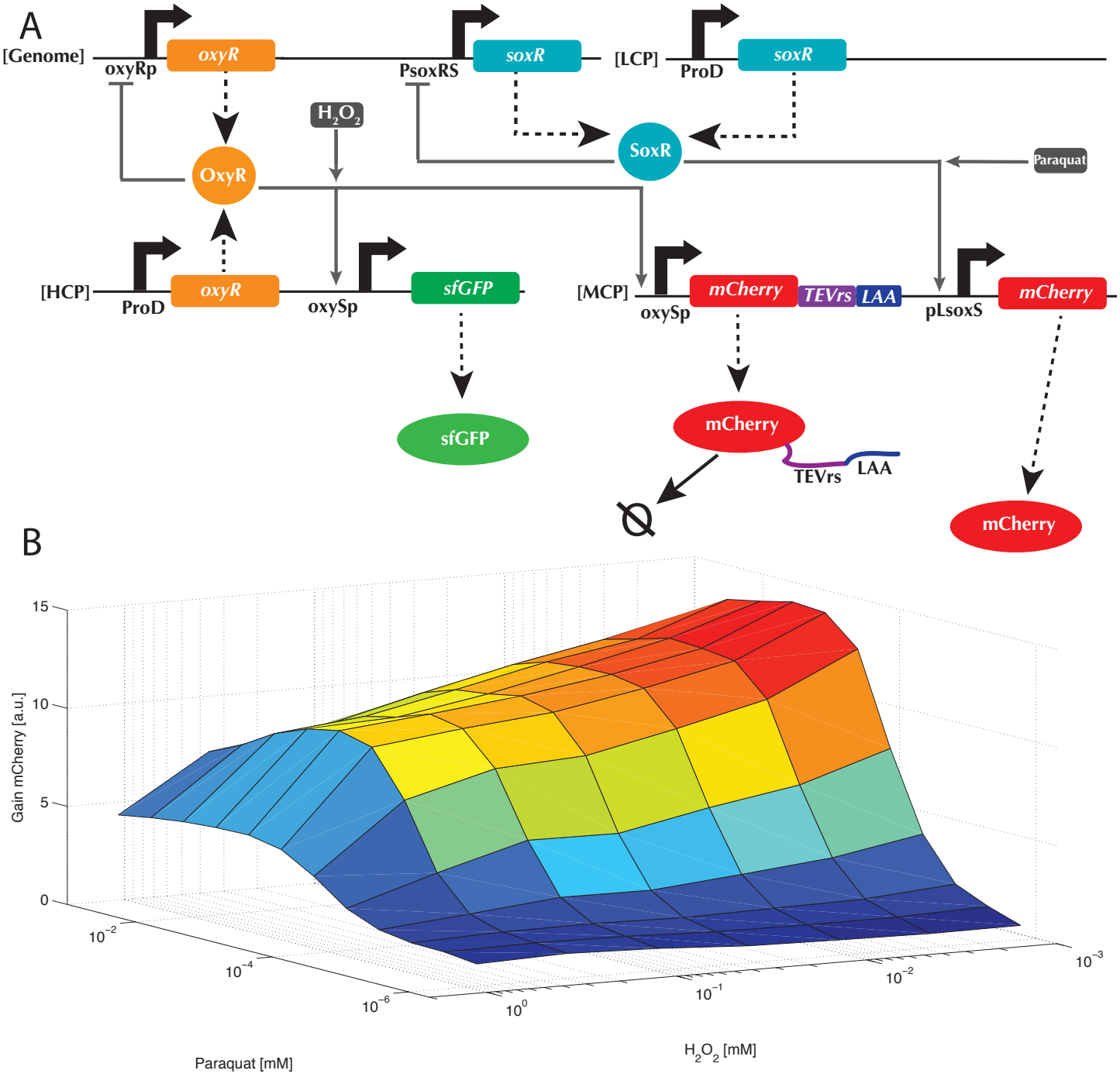

Supplementary Figure 9 | The dual-sensor circuit with the variable-analog compensation circuit without TEVp. (A) The dual-sensor circuit with the variable-analog compensation circuit without pLsoxS-*TEVp*. mCherry expressed from oxySp is targeted for degradation due to the LAA degradation signal. **(B)** The mCherry output from the circuit in (A) in terms of fold-change relative to minimum fluorescence. Because oxySp-derived mCherry is rapidly degraded, the mCherry output looks similar to the first iteration of the dual-ROS sensing circuit (Fig. 3B). The data are derived from three biological replicates and flow cytometry experiments, each involving 30,000 events. The lowest concentrations of paraquat and H_2O_2 tested were zero, but are plotted as non-zero numbers so as to be shown on the logarithmic axes. Source data are provided as a Source Data file.

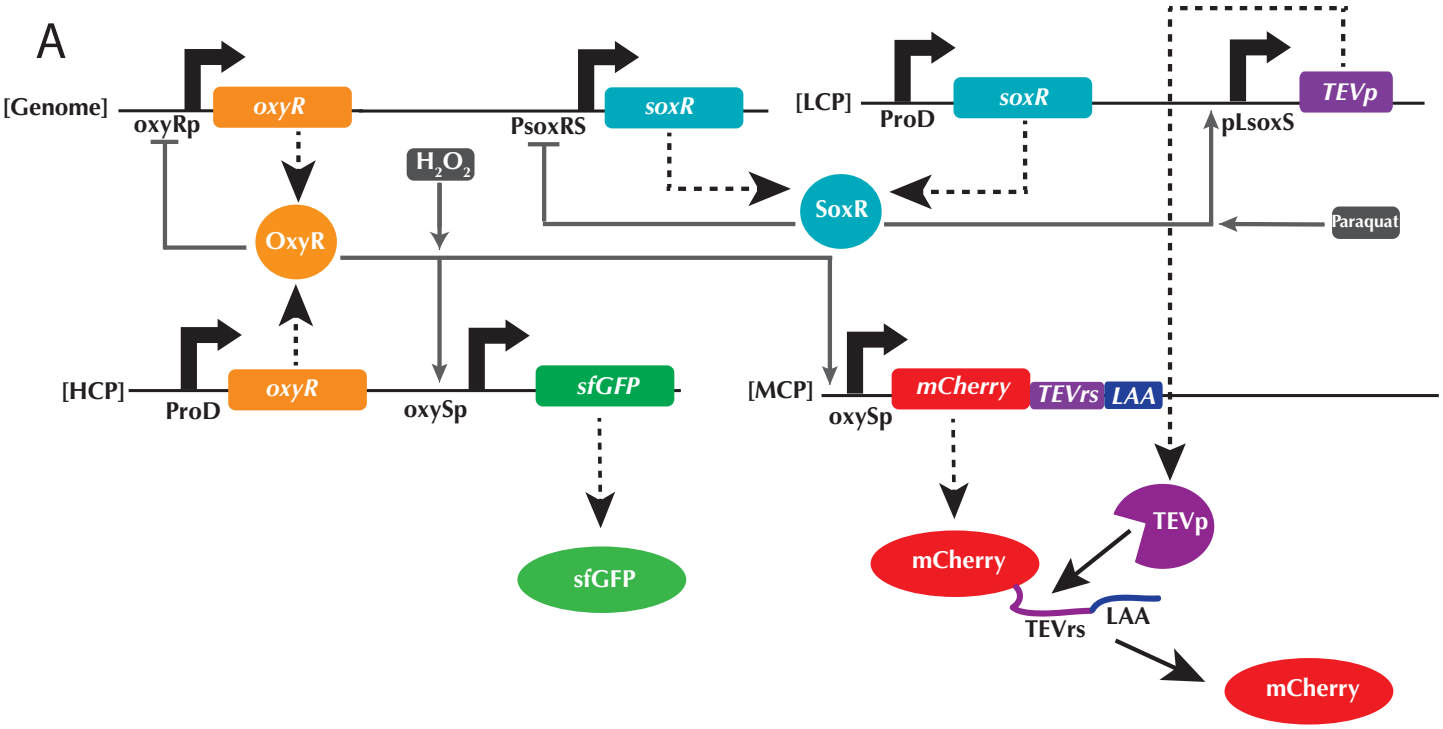
A
[Genome]
oxyRp
oxyR
PsoxRS
soxR
[LCP]
ProD
soxR
pLsoxS
TEVp
H2O2
OxyR
SoxR
Paraquat
[HCP]
ProD
oxyR
oxySp
sfGFP
[MCP]
oxySp
mCherry
TEVrs
LAA
sfGFP
TEVp
mCherry
TEVrs
LAA
mCherry

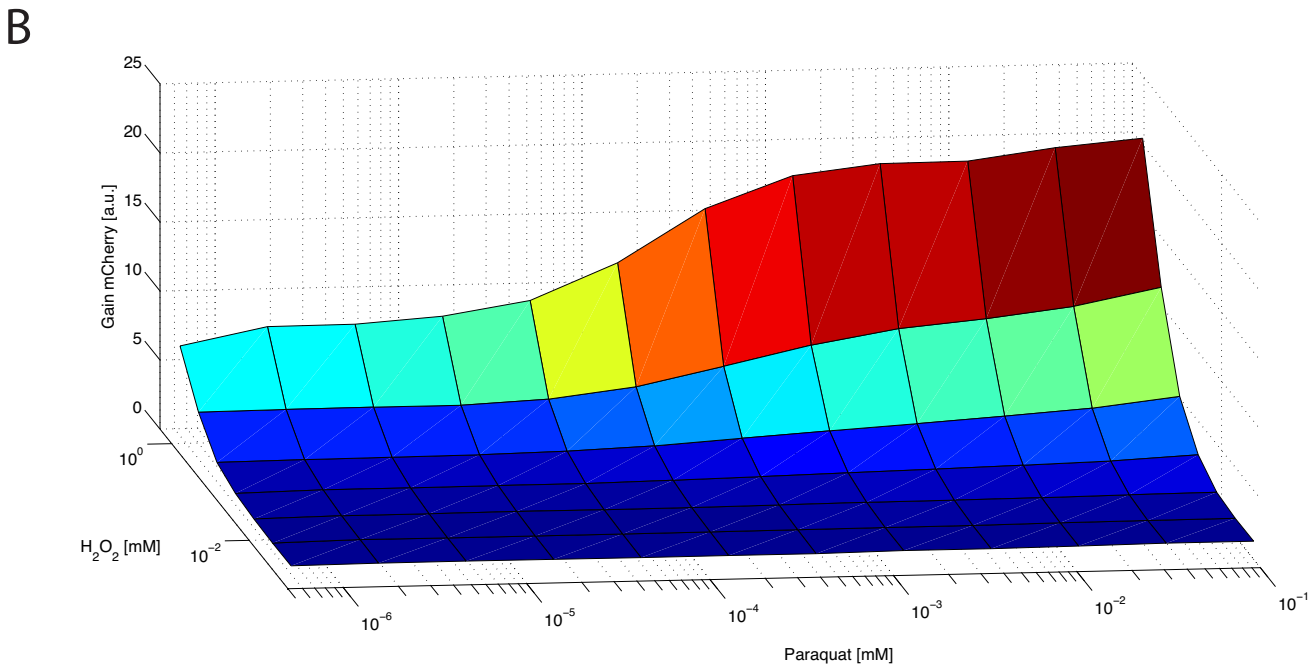
B
Gain mCherry [a.u.]
25
20
15
10
5
0
H2O2 [mM]
10^0
10^-2
10^-6
10^-5
10^-4
10^-3
10^-2
10^-1
Paraquat [mM]

C

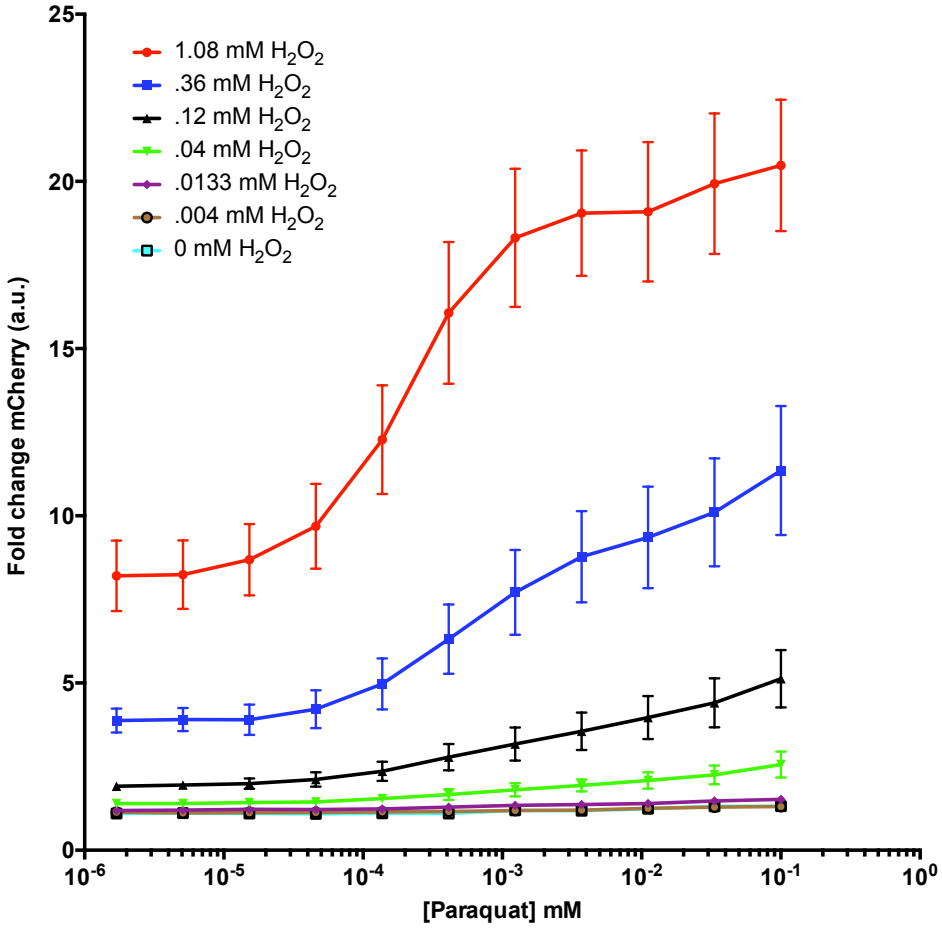

Supplementary Figure 10 | The dual-sensor circuit with the variable-analog compensation circuit without pLsoxS-mCherry. (A) In order to characterize the effect of the variable-analog compensation circuit on mCherry expression independently from the SoxR-based system, we removed the pLsoxS-mCherry operon so that mCherry was only expressed from the oxySp promoter. **(B)** The mCherry output in terms of fold-change relative to minimum fluorescence. The "compensation" function of the variable-analog compensation circuit resembles the raw mCherry error for the dual-sensor circuit (Supplementary Fig. 6). The lowest concentrations of paraquat and H_2O_2 tested were zero, but are plotted as non-zero numbers so as to be shown on the logarithmic axes. **(C)** The mCherry output from Supplementary Fig. 10B in terms of fold-change of mCherry expression versus paraquat concentration at different concentrations of H_2O_2. The errors (s.e.m.) are derived from three biological replicates and flow cytometry experiments, each involving 30,000 events. Source data are provided as a Source Data file.

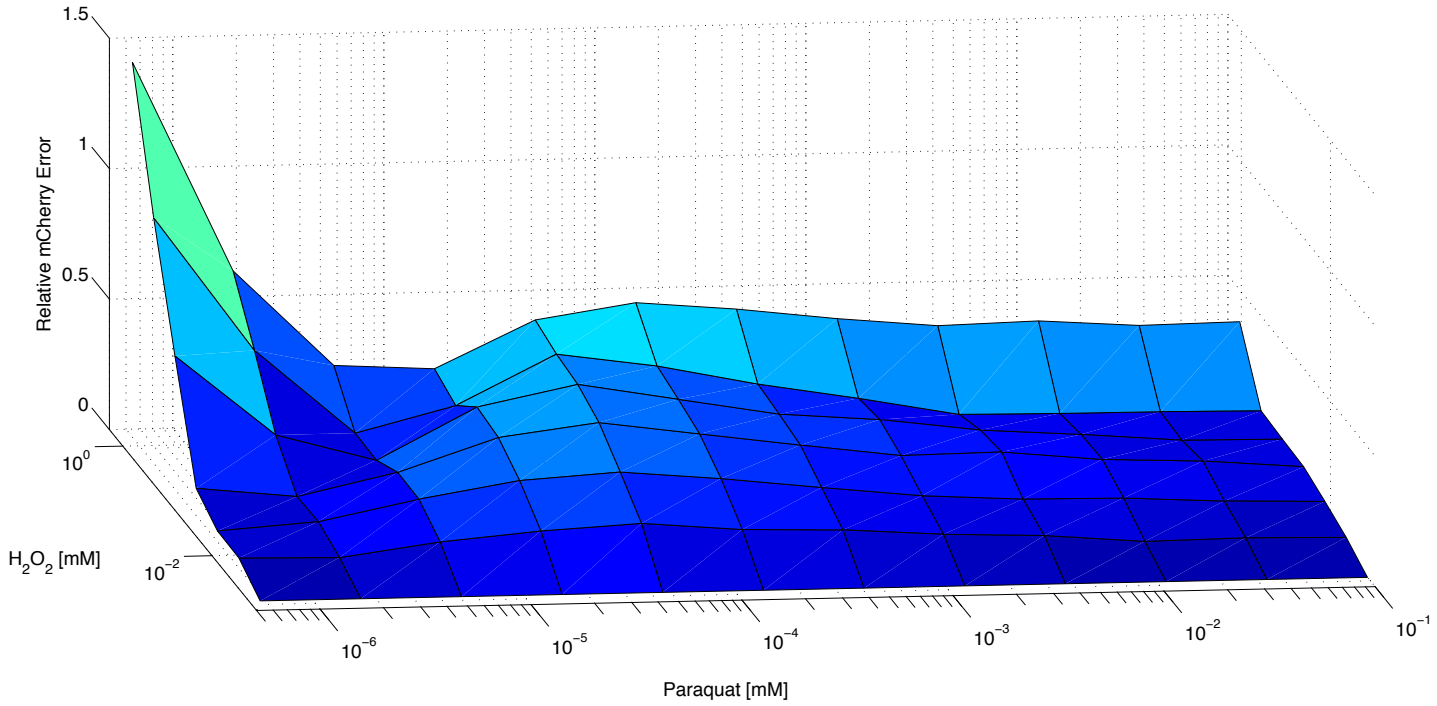

Supplementary Figure 11 | Relative mCherry error for the dual-sensor circuit with the variable-analog compensation circuit (Fig. 3E) based on the data in Fig. 3F. Crosstalk is lower at high paraquat levels and is reduced at low paraquat compared to the initial dual-sensor circuit in Supplementary Fig. 7. The data shown is the mean of the relative error calculated from each experimental replicate. The lowest concentrations of paraquat and H_2O_2 tested were zero, but are plotted as non-zero numbers so as to be shown on the logarithmic axes.

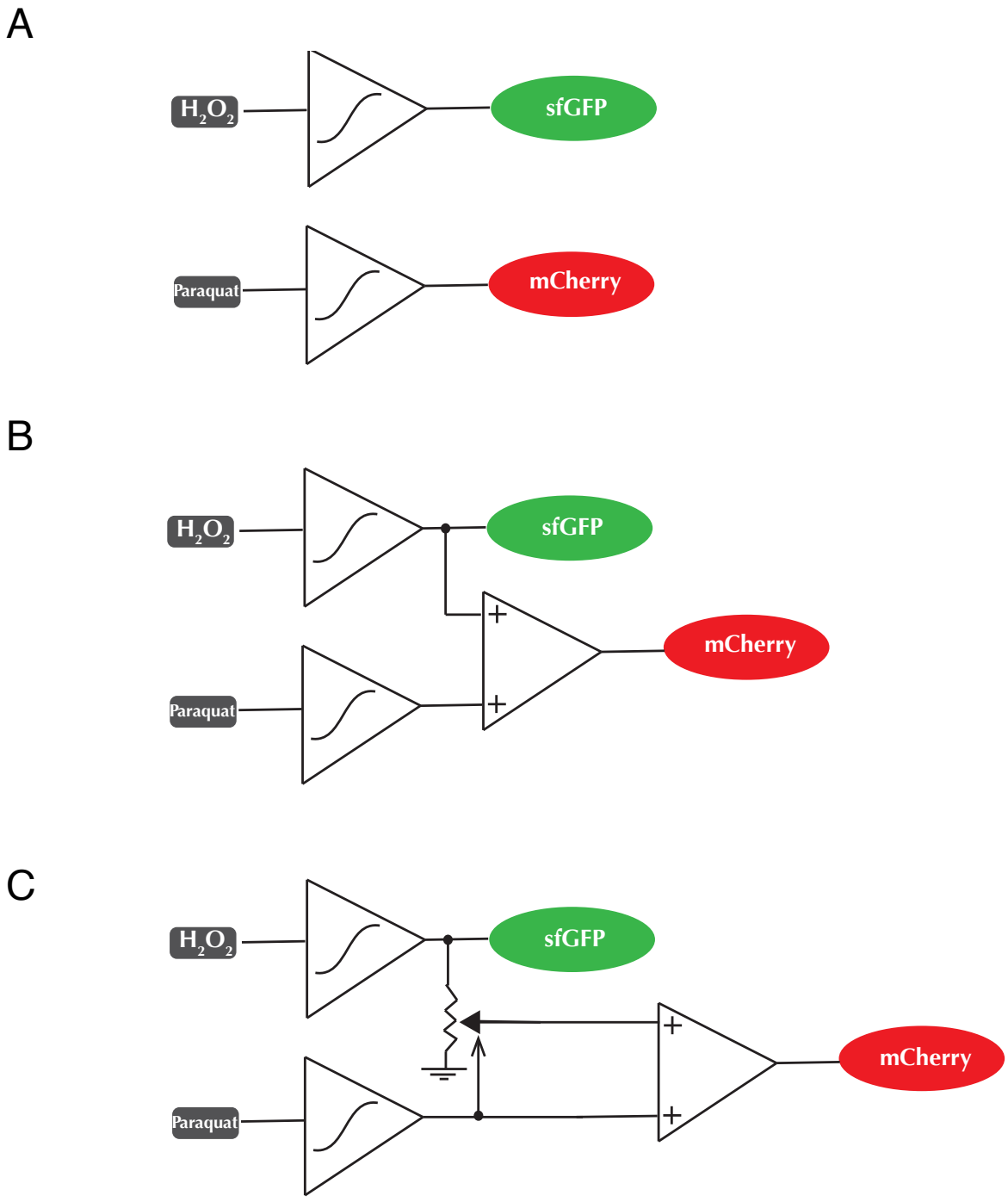

Supplementary Figure 12 | Abstraction of dual-sensor strains. (A) The first iteration of the dual-sensor circuit in Fig. 3A. The sfGFP output is dependent upon H_2O_2 input concentration and the mCherry output is dependent upon paraquat input concentration. **(B)** The dual-sensor circuit with the analog compensation circuit. The sfGFP output is dependent upon H_2O_2 input concentration. The total mCherry output is the sum of mCherry resulting from the H_2O_2-sensing circuit and the paraquat-sensing circuit. **(C)** The dual-sensor circuit with the variable-analog compensation circuit. The sfGFP output is dependent upon H_2O_2 input concentration. The total mCherry output is the sum of mCherry resulting from the H_2O_2-sensing circuit and the paraquat-sensing circuit, where the paraquat-sensing circuit can adjust the amount of mCherry resulting from the H_2O_2-sensing circuit by adjusting the mCherry degradation rate. We describe this scenario as being conceptually analogous to a potentiometer whose output can be regulated by a paraquat circuit.

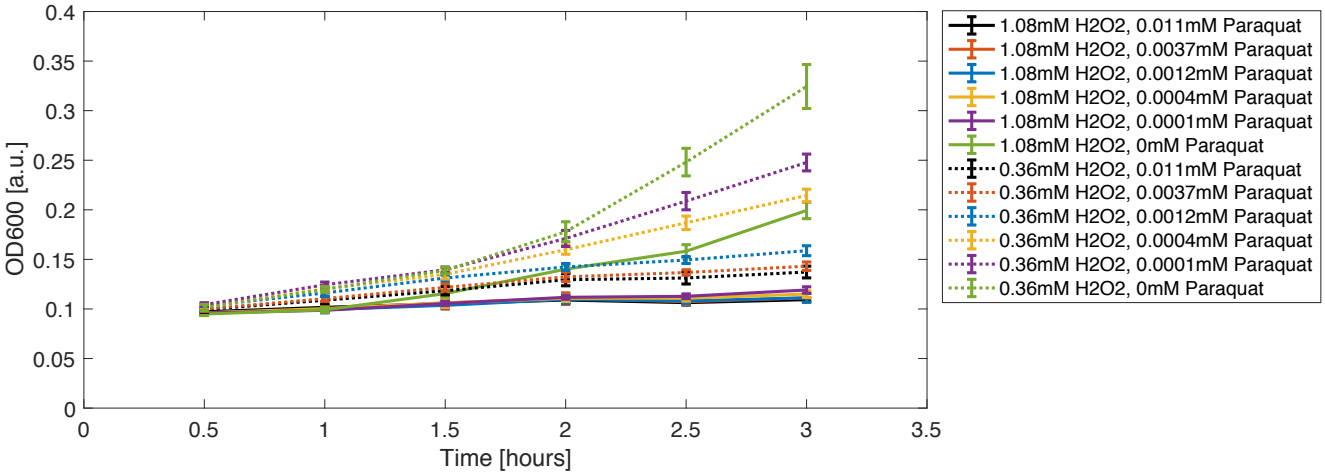

Supplementary Figure 13 | Growth of the dual-sensor strain in the presence of combinations of high concentrations of ROS. The dual-sensor strain (Fig. 3A) was exposed to different combinations of high concentrations of paraquat and H_2O_2, and growth was assayed every 30 minutes up to 3 hours by measuring the optical density of the culture at 600 nM. 1.08 mM H_2O_2 repressed cell growth to a negligible rate in the presence of paraquat. The mean and error (s.d.) shown are calculated from replicates (n=8) derived from the same parent culture. Source data are provided as a Source Data file.

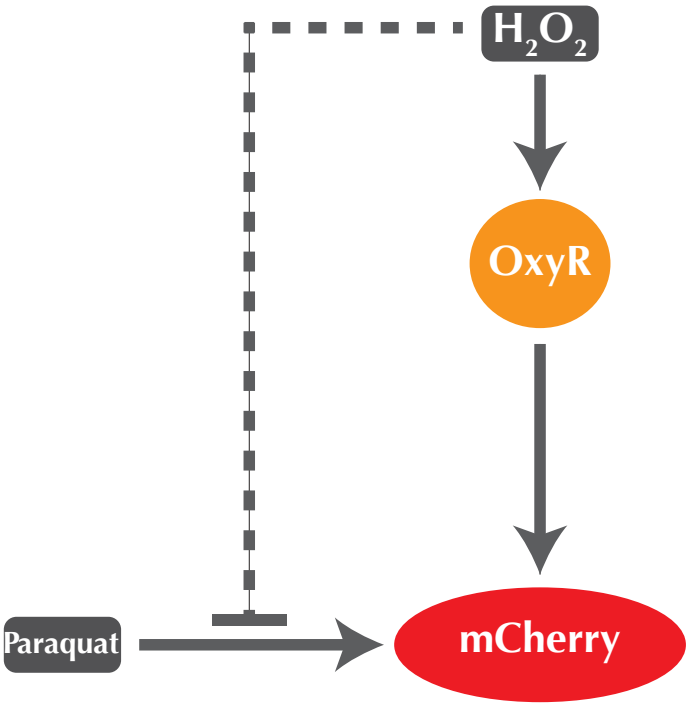

Supplementary Figure 14 | Incoherent feedforward loop in crosstalk compensation. H_2O_2 represses mCherry expression when paraquat is present via unknown crosstalk mechanisms (dashed line) and activates mCherry expression via a transcriptional connection through OxyR. The net result is that the effect of H_2O_2 on mCherry expression is little.


pLlacO
RBS0030
oxyR
TermT1
p15A
TermT0
KanR
fIM1264
pZA2-pLlacO-oxyR


oxySp
RBS0030
mCherry
TermT1
ColE1
TermT0
AmpR
TJF117
pZE1-oxySp-mCherry


katGp
RBS0030
mCherry
TermT1
ColE1
TermT0
AmpR
TJF64
pZE1-katGp-mCherry


ahpCp
RBS0030
mCherry
TermT1
ColE1
TermT0
AmpR
TJF66
pZE1-ahpCp-mCherry

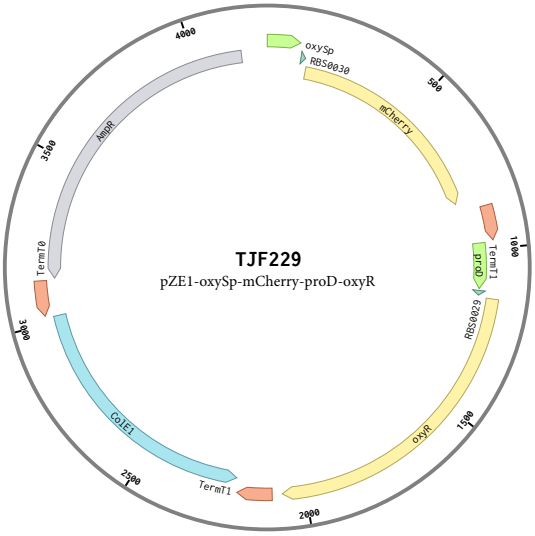
oxySp
RBS0030
mCherry
TermT1
prod
RBS0023
oxyR
TermT1
ColE1
TermT0
AmpR
TJF229
pZE1-oxySp-mCherry-proD-oxyR

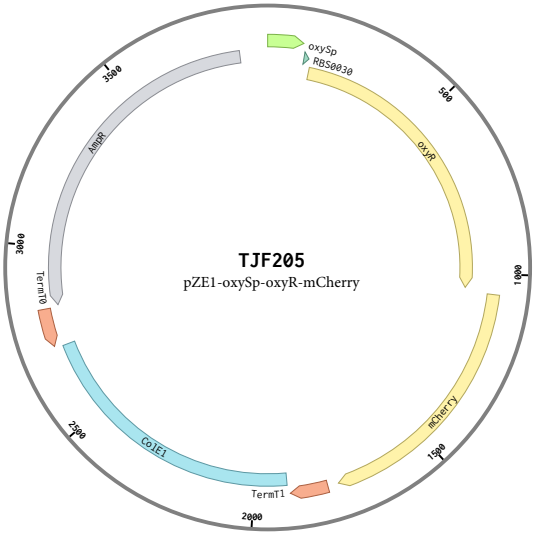
oxySp
RBS0030
oxyR
mCherry
TermT1
ColE1
TermT0
AmpR
TJF205
pZE1-oxySp-oxyR-mCherry


pLlacO
RBS0030
soxR
TermT1
p15A
TermT0
KanR
fIM1265
pZA2-pLlacO-soxR

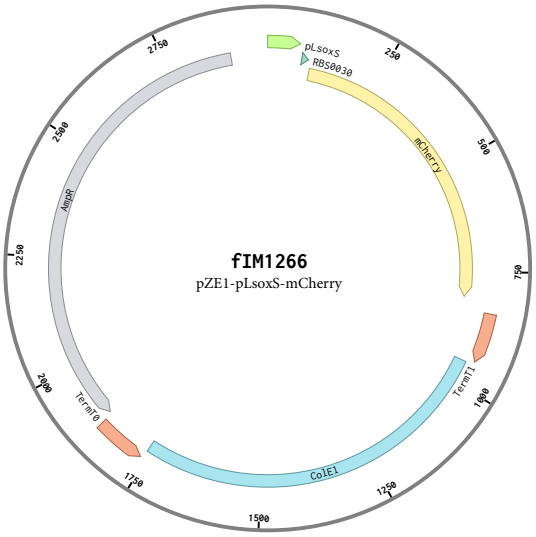
pLsoxS
RBS0030
mCherry
TermT1
ColE1
TermT0
AmpR
fIM1266
pZE1-pLsoxS-mCherry


pLsoxS
RBS0030
soxR
mCherry
TermT1
ColE1
TermT0
CmR
JRF145
pZE3-pLsoxS-soxR-mCherry

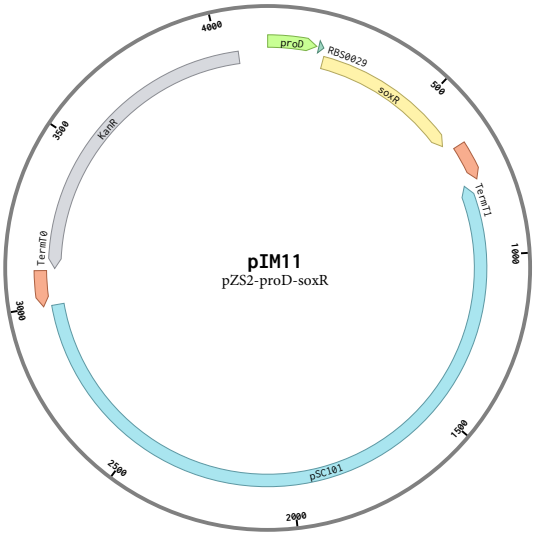
proD
RBS0029
soxR
TermT1
pSC101
TermT0
KanR
pIM11
pZS2-proD-soxR


pLsoxS
RBS0030
mCherry
TermT1
p15A
TermT0
SpecR
pIM10
pZA4-pLsoxS-mCherry

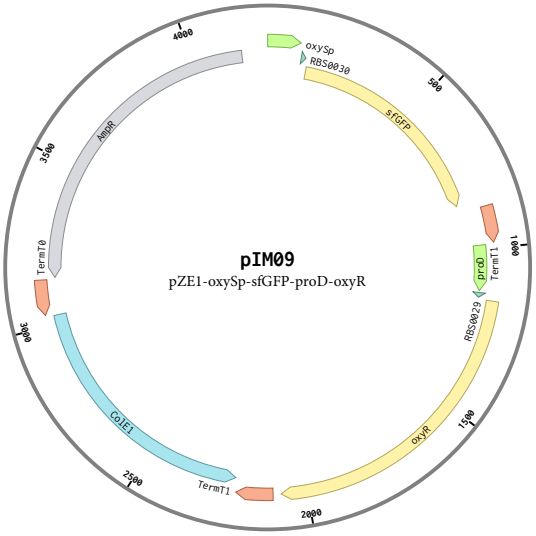
oxySp
RBS0030
sfGFP
TermT1
proD
RBS0029
oxyR
TermT1
ColE1
TermT0
AmpR
pIM09
pZE1-oxySp-sfGFP-proD-oxyR

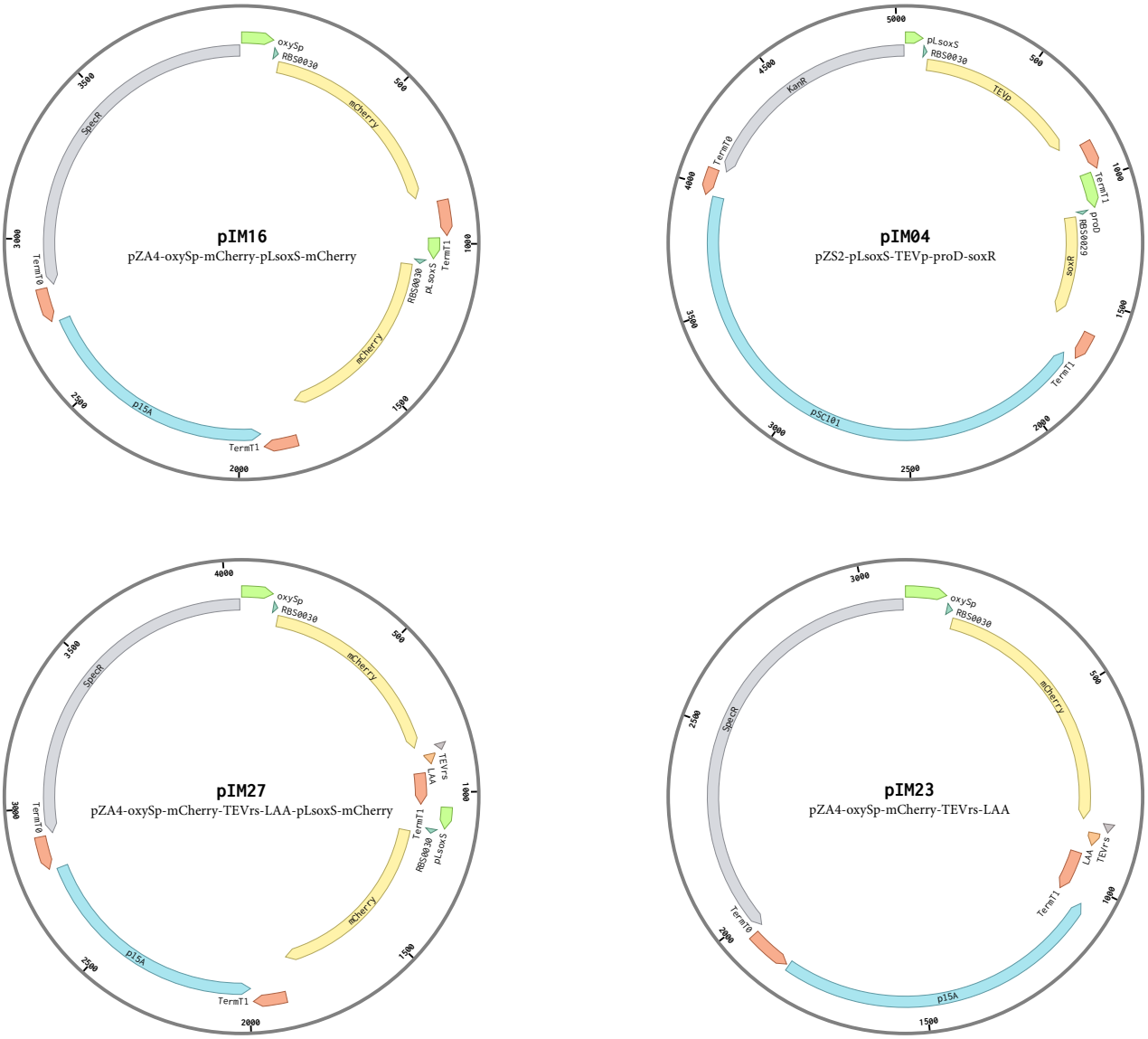

Supplementary Figure 15 | Plasmid maps used in this study.

Supplementary Table 1 | List of plasmids used in experiments

Name	Description	Figure
fIM1264	pZA2-pLlacO-oxyR	Fig. 1A
TJF117	pZE1-oxySp-mCherry	Fig. 1A
TJF64	pZE1-katGp-mCherry	Fig. 1A
TJF66	pZE1-ahpCp-mCherry	Fig. 1A
TJF229	pZE1-oxySp-mCherry-proD-oxyR	Fig. 1D
TJF205	pZE1-oxySp-oxyR-mCherry	Fig. 1E
fIM1265	pZA2-pLlacO-soxR	Figs. 2A, 2E
fIM1266	pZE1-pLsoxS-mCherry	Figs. 2A, 2E
JRF145	pZE3-pLsoxS-soxR-mCherry	Fig. 2B
pIM11	pZS2-proD-soxR	Figs. 3A, 3C, Supplementary Fig. 9A
pIM10	pZA4-pLsoxS-mCherry	Fig. 3A
pIM09	pZE1-oxySp-sfGFP-proD-oxyR	Figs. 3A, 3C, 3E, Supplementary Figs. 9A, 10A
pIM16	pZA4-oxySp-mCherry-pLsoxS-mCherry	Fig. 3C
pIM04	pZS2-pLsoxS-TEVp-proD-soxR	Fig. 3E, Supplementary Fig. 10A
pIM27	pZA4-oxySp-mCherry-TEVrs-LAA-pLsoxS-mCherry	Fig. 3E, Supplementary Fig. 9A
pIM23	pZA4-oxySp-mCherry-TEVrs-LAA	Supplementary Fig. 10A

Supplementary Table 2 | List of synthetic parts

Part Name	Description and Source
pLlacO	pLlacO-1 LacI-repressible promoter (3)
pLsoxS	The *soxS* promoter SoxR-binding site fused to lambda phage promoter -10 and -35 sequences (4)
oxySp	Promoter for *E. coli oxySp* RNA (5)
katGp	Promoter for *E. coli katG* gene (5)
ahpCp	Promoter for *E. coli ahpC* gene (5)
proD	Strong proD promoter (6)
RBS0030	Ribosome binding site. BBa_B0030 (7)
RBS0029	Ribosome binding site. BBa_B0029 (7)
oxyR	*oxyR* protein-coding sequence (5)
soxR	*soxR* protein-coding sequence (5)
TEVp	TEV protease protein-coding sequence (8)
mCherry	mCherry fluorescent protein coding sequence. BBa_J06504 (7)
sfGFP	Super-folder green fluorescent protein coding sequence. BBa_I746916 (7)
TEVrs	TEV protease recognition sequence (9)
LAA	LAA degradation tag (7)
TermT1	Terminator T1 (3*)*
TermT0	Terminator T0 (3)
p15A	Medium-copy number origin of replication (3)
ColE1	High-copy number origin of replication (3)
pSC101	Low-copy number origin of replication (3)
ampR	Ampicillin-resistance cassette (3)
kanR	Kanamycin-resistance cassette (3)
specR	Spectinomycin-resistance cassette (3)
cmR	Chloramphenicol-resistance cassette (3)

Supplementary Note 1: Calculating output fold-induction, relative input range, sensitivity, and utility

1. Calculate best-fitting Hill function from the raw data:

   Hill functions are of the form:

$$y = \frac{b_{max} * x^n}{{K_d}^n + x^n} + C$$

   Where C is the empirical geometric mean (y) at zero input (x = 0), and n, K_d, and b_{max} are fit to the data.

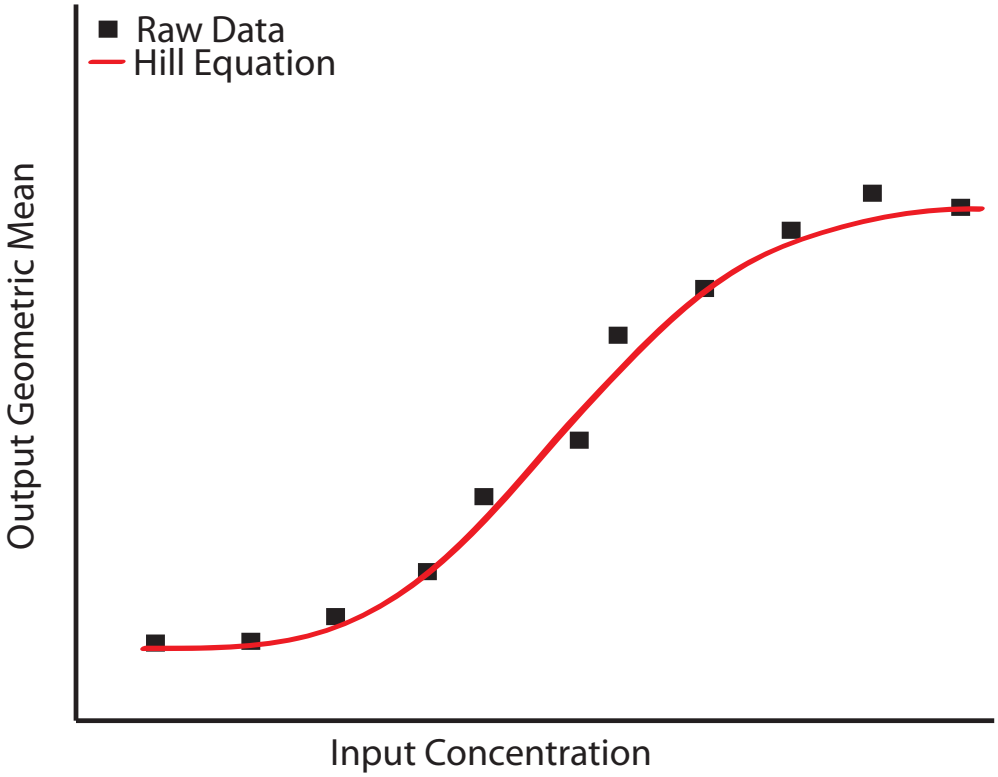

2. Calculate the output fold-induction (FI):

$$FI = \frac{(b_{max} + C)}{C}$$

   If the observed maximum gene expression is less than the theoretical maximum gene expression ($b_{max} + C$), then the observed maximum gene expression ($b_{max,\ observed}$) is used to calculate the output fold-induction. In this case, the output fold-induction is:

$$FI = \frac{(b_{max,observed})}{C}$$

3. Calculate the Input Dynamic Range (*10*):

A) In the case where the theoretical b_{max} is less than the maximum gene expression observed:

90% of maximum output (Y_{90}) is calculated as:

$$Y_{90} = C + .9 * b_{max}$$

10% of maximum output (Y_{10}) is calculated as:

$$Y_{10} = C + .1 * b_{max}$$

Y_{90} and Y_{10} are interpolated to the X-axis using the Hill function to determine X_{90} and X_{10}.

The input concentration for 90% of the maximum output (X_{90}) is calculated as:

$$X_{90} = K_d * \sqrt[n]{9}$$

The input concentration for 10% of the maximum output (X_{10}) is calculated as:

$$X_{10} = \frac{K_d}{\sqrt[n]{9}}$$

The relative input range (RIR) is calculated as:

$$RIR = \frac{X_{90}}{X_{10}} = \sqrt[n]{81}$$

B) In the case where the theoretical b_{max} is greater than the max gene expression observed:

90% of maximum output (Y_{90}) is calculated as:

$$Y_{90} = C + .9 * (b_{max,observed} - C)$$

10% of maximum output (Y_{10}) is calculated as:

$$Y_{10} = C + .1 * (b_{max,observed} - C)$$

Y_{90} and Y_{10} are interpolated to the X-axis using the Hill function to determine X_{90} and X_{10}.

The input concentration for 90% of the maximum output (X_{90}) is calculated as:

$$X_{90} = K_d * \sqrt[n]{\frac{b_{max,observed} - C}{\frac{10}{9} * b_{max} + C - b_{max,observed}}}$$

The input concentration for 10% of the maximum output (X_{10}) is calculated as:

$$X_{10} = K_d * \sqrt[n]{\frac{b_{max,observed} - C}{10 * b_{max} + C - b_{max,observed}}}$$

The relative input range (RIR) is calculated as:

$$RIR = \frac{X_{90}}{X_{10}} = \sqrt[n]{\frac{10 * b_{max} + C - b_{max,observed}}{\frac{10}{9} * b_{max} + C - b_{max,observed}}}$$

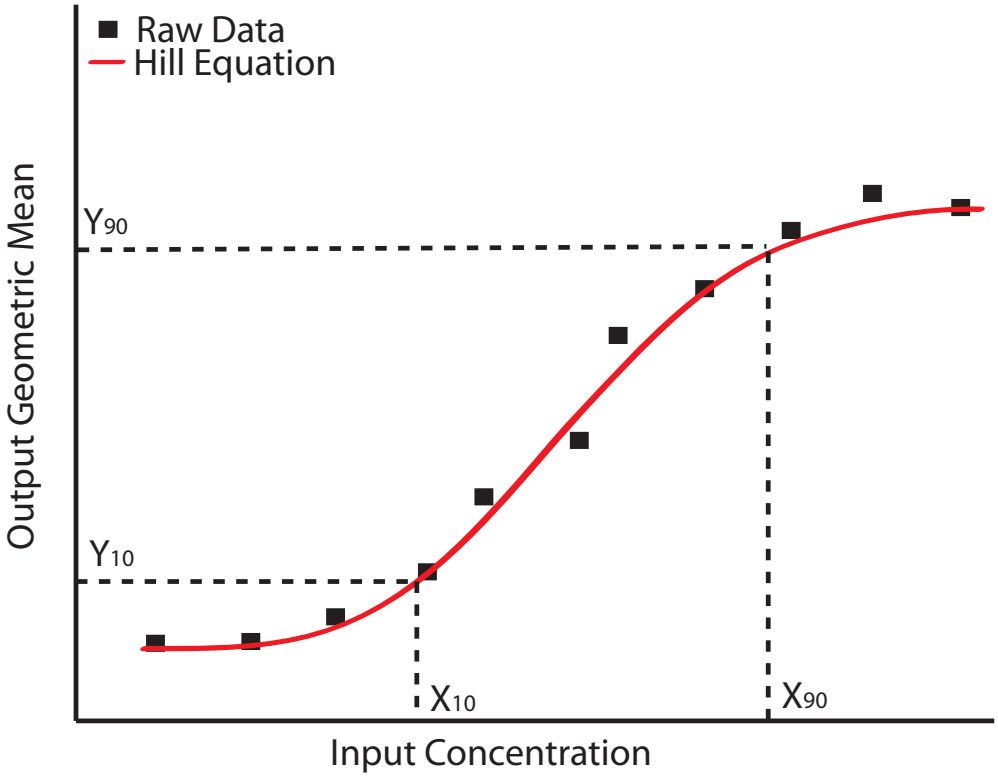

4. Calculate utility by multiplying the relative input dynamic range by the output fold-induction:

$$Utility = FI * RIR$$

Supplementary Note 2: Calculating errors due to crosstalk between circuits

1. Calculate the raw error:

   In the ideal scenario for the circuits from Fig. 3, mCherry expression should only be controlled by the input paraquat concentration. To determine the raw error in mCherry expression, we subtracted the mCherry level at every given concentration of paraquat and H_2O_2 from the mCherry level at the same concentration of paraquat but with zero H_2O_2.

   $$Raw\ error = GeneExpression_{paraquat_a,\ H_2O_2\ b} - GeneExpression_{paraquat_a,\ H_2O_2\ 0}$$

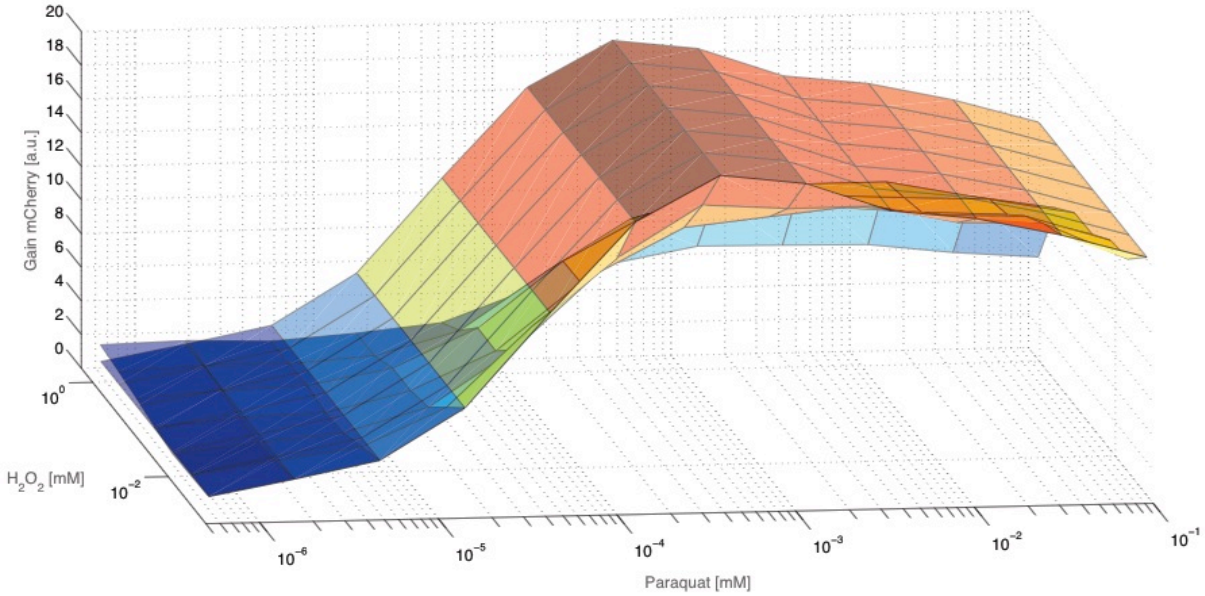

   In the figure above, mCherry expression across a range of paraquat concentrations and zero H_2O_2 is extrapolated and overlaid on top of mCherry expression across the entire range of paraquat and H_2O_2 concentrations. The difference between these two mCherry levels is the raw error. The raw error for a single experimental replicate for the circuit in Fig. 3A is shown below. The lowest concentrations of paraquat and H_2O_2 tested were zero, but are plotted as non-zero numbers so as to be shown on the logarithmic axes.

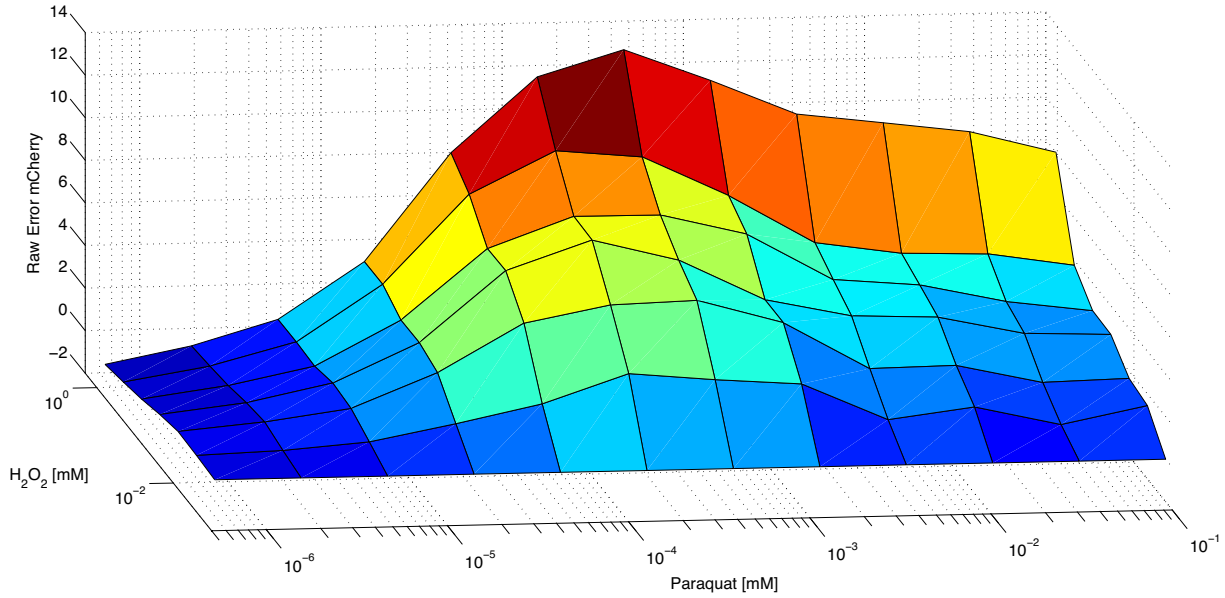

2. Calculate the absolute error:

   The absolute error is calculated by taking the absolute value of the raw error. The absolute error for a single experimental replicate for the circuit in Fig. 3A is shown below. The lowest concentrations of paraquat and H_2O_2 tested were zero, but are plotted as non-zero numbers so as to be shown on the logarithmic axes.

$$Absolute\ error = \left| GeneExpression_{paraquat_a,\ H_2O_2\ b} - GeneExpression_{paraquat_a,\ H_2O_2\ 0} \right|$$

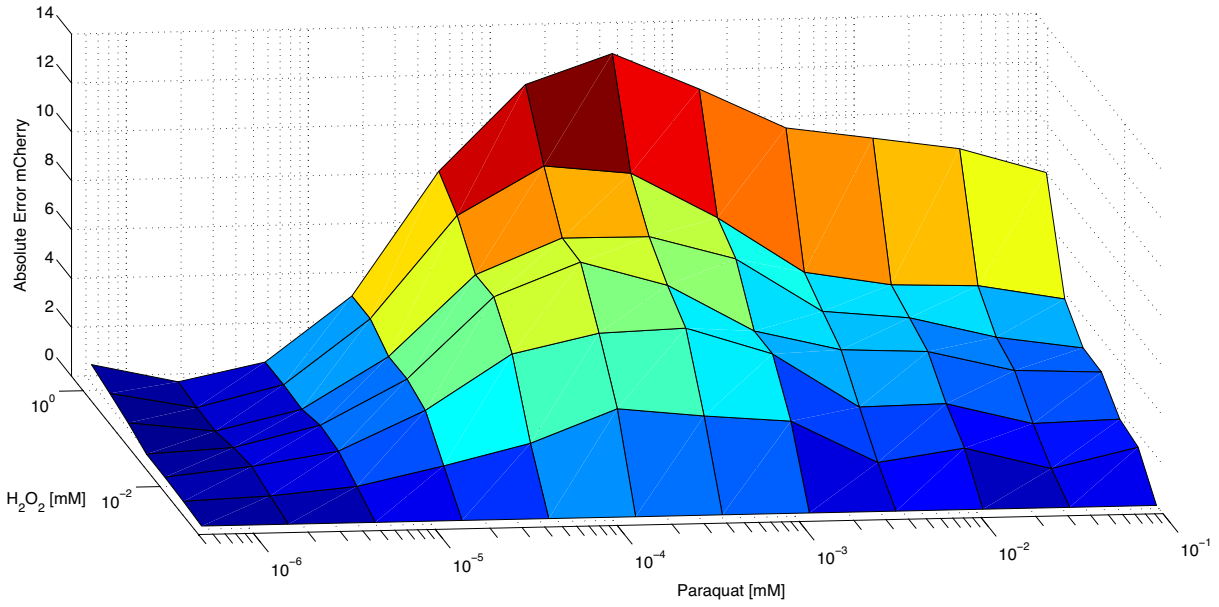

3. Calculate the relative error:

   The relative error is calculated by normalizing the absolute error to the corresponding mCherry level at the same concentration of paraquat but with zero H_2O_2. The relative error for an experimental replicate for the circuit in Fig. 3A is shown below. The lowest concentrations of paraquat and H_2O_2 tested were zero, but are plotted as non-zero numbers so as to be shown on the logarithmic axes.

$$Relative\ error = \frac{\left| GeneExpression_{paraquat_a,\ H_2O_2\ b} - GeneExpression_{paraquat_a,\ H_2O_2\ 0} \right|}{GeneExpression_{paraquat_a,\ H_2O_2\ 0}}$$

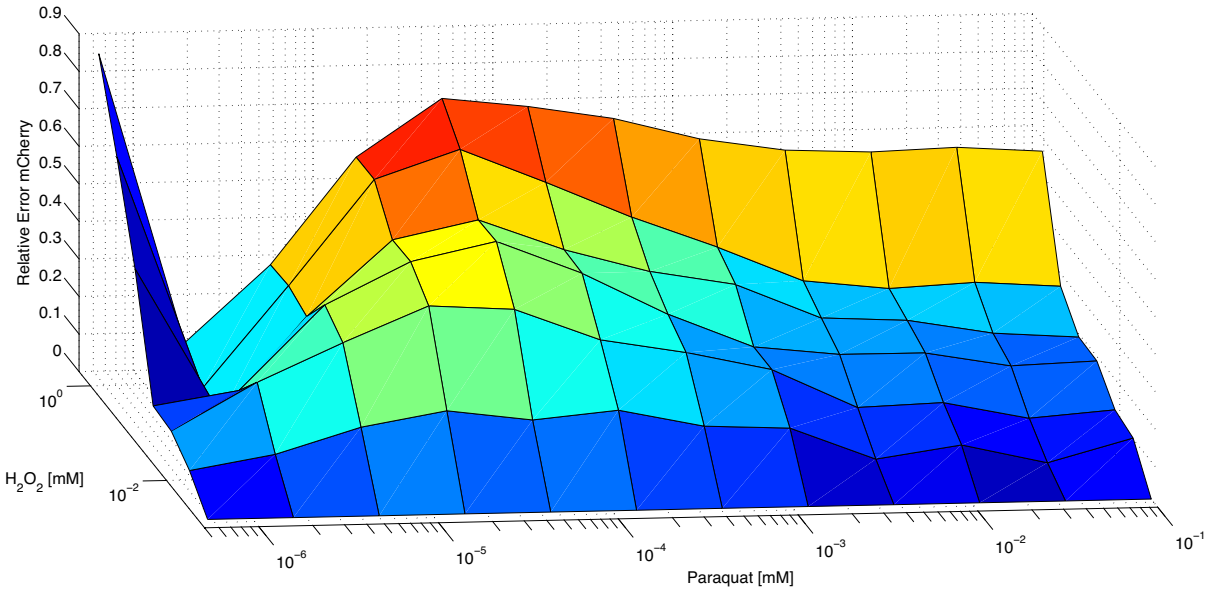

4. Sum the relative errors to get the total relative error:

   To calculate the total relative error, the relative error at every concentration of paraquat and H_2O_2 is summed.

$$Total\ relative\ error =$$

$$\sum_{paraquat_0,\ H_2O_2\ 0}^{paraquat_{max},\ H_2O_2\ max} \frac{\left|GeneExpression_{paraquat_a,\ H_2O_2\ b} - GeneExpression_{paraquat_a,\ H_2O_2\ 0}\right|}{GeneExpression_{paraquat_a,\ H_2O_2\ 0}}$$

   This procedure for calculating errors has been illustrated for the mCherry output of a single experimental replicate of the circuit shown in Fig. 3A. The analogous procedure can be carried out for the sfGFP output of the circuits in Fig. 3, thus resulting in the calculations plotted in Fig. 3I.

Supplementary References

1. Shibata, T. & Fujimoto, K. Noisy signal amplification in ultrasensitive signal transduction. *Proc. Natl. Acad. Sci. USA* **102**, 331-336 (2005).
2. Hidalgo, E., Leautaud, V. & Demple, B. The redox-regulated SoxR protein acts from a single DNA site as a repressor and an allosteric activator. *EMBO J.* **17**, 2629-2636 (1998).
3. Lutz, R. & Bujard, H. Independent and tight regulation of transcriptional units in *Escherichia coli* via the LacR/O, the TetR/O and AraC/I_1-I_2 regulatory elements. *Nucleic Acids Res.* **25**, 1203-1210 (1997).
4. Dwyer, D. J., Kohanski, M. A., Hayete, B. & Collins, J. J. Gyrase inhibitors induce an oxidative damage cellular death pathway in *Escherichia coli*. *Mol. Syst. Biol.* **3**, 91 (2007).
5. The EcoCyc Database, (available at http://ecocyc.org/).
6. Davis, J. H., Rubin, A. J. & Sauer, R. T. Design, construction and characterization of a set of insulated bacterial promoters. *Nucleic Acids Res.* **39**, 1131-1141 (2011).
7. Registry of Standard Biological Parts, (available at http://igem.org/registry).
8. Kapust R. B. et al. Tobacco etch virus protease: mechanism of autolysis and rational design of stable mutants with wild-type catalytic proficiency. *Protein Eng.* **14**, 993-1000 (2001).
9. Kostallas, G., Löfdahl, P. Å. & Samuelson, P. Substrate Profiling of Tobacco Etch Virus Protease Using a Novel Fluorescence-Assisted Whole-Cell Assay. *PLoS ONE* **6**, e16136 (2011).
10. Madar, D., Dekel, E., Bren, A. & Alon, U. Negative auto-regulation increases the input dynamic-range of the arabinose system of *Escherichia coli*. *BMC Syst. Biol.* **5**, 111 (2011).